New Mexico Scintillometer Network in Support of Remote Sensing, and Hydrologic and Meteorological Models

Jan Kleissl[1], Sung-ho Hong[2], and Jan M.H. Hendrickx[2]
[1] Dept of Mechanical & Aerospace Eng., University of California, San Diego, (previously at New Mexico Tech), 9500 Gilman Dr. 0411, La Jolla, CA 92093-0411, jkleissl@ucsd.edu, ph: 443 527 2740
[2] Dept of Earth & Environmental Sciences, New Mexico Tech, 801 Leroy Place, Socorro, NM 87801, USA

Abstract

In New Mexico, a first-of-its-kind network of seven Large Aperture Scintillometer (LAS) sites was established in 2006 to measure sensible heat fluxes over irrigated fields, riparian areas, deserts, lava flows, and mountain highlands. Wireless networking infrastructure and auxiliary meteorological measurements facilitate real-time data assimilation. LAS measurements are advantageous in that they vastly exceed the footprint size of commonly used ground measurements of sensible and latent heat fluxes (~100 m^2), matching the pixel-size of satellite images or grid cells of hydrologic and meteorological models (~0.1-5 km^2). Consequently, the LAS measurements can be used to validate, calibrate, and force hydrologic, remote sensing, and weather forecast models. Initial results are presented for: (1) variability and error of sensible heat flux measurements by scintillometers over heterogeneous terrain and (2) the validation of the Surface Energy Balance Algorithm for Land (SEBAL) applied to MODIS satellite imagery. Findings from this study are discussed in the context of researchers' and practitioners' data assimilation needs.

Capsule

Large Aperture Scintillometers have been successfully used in a variety of ecosystems in New Mexico to measure sensible heat fluxes at the km scale.

Sustainable management of water resources in arid and semi-arid watersheds requires accurate information on consumptive water use over a range of space and time scales. Consumptive water use by grasses and shrubs, irrigated crops, and riparian vegetation in desert regions is highly variable in space and time. The spatial variability is caused by the heterogeneous nature of vegetation cover, hydraulic soil properties, ground water table depths, and differences in water availability caused by hydrological processes. The temporal variability is caused by daily and seasonal changes in weather conditions, availability of stored soil water, and root extraction. In the southwestern US evapotranspiration is the major flux exiting the watersheds and represents typically more than half of the total depletion (Middle Rio Grande Water Council, 1999). Moreover, in water balance computations, at watershed scales, evapotranspiration (ET) is the component with the least amount of certainty (Goodrich et al., 2000).

During the last two decades many investigators have explored the application of satellite optical (i.e. visible, near- and mid-infrared, thermal infrared) remote sensing for the estimation of regional ET distributions (Choudhury, 1989; Kustas and Norman, 1996; Moran and Jackson, 1991). These efforts have resulted in the development of several operational remote sensing ET algorithms that are now being used by researchers and practitioners. Examples are: SEBAL (Surface Energy Balance Algorithms for Land, Bastiaanssen et al. 1998, as applied in New Mexico by Hendrickx and Hong, 2005), METRIC™ (Mapping ET at high spatial Resolution with Internalized Calibration, Allen et al. 2006), ALEXI (Anderson et al., 2004), NLDAS and LIS (Peters Lidard et al., 2004), and PASS (Song et al. 2000). Although these algorithms are quite different in their spatial and temporal scales (30 m to 1/8th degree or about 13 km in New Mexico, daily to monthly), they all have produced ET maps on local, regional, or national scales that are being used successfully by hydrologists and water resources professionals.

In addition to the visible, near-infrared and mid-infrared bands, the thermal IR (TIR) band is critical for the estimation of ET from satellite images. The spatial resolution of Landsat satellite TIR remote sensing images varies from 60 m on Landsat7 to 120 m on Landsat5 (Fig. 1), but these images are impracticable for continuous operation of hydrologic remote sensing algorithms due to their infrequent coverage (biweekly or longer under cloudy conditions). Satellites with daily global coverage (MODIS, AVHRR, and NPOESS in the future) capture thermal images with a spatial resolution of about 1000 m. Hydrologic and numerical weather prediction (NWP) models have even larger grid scales. For example, the NWS North American Model (NAM) is operational at 12 km resolution but efforts are under way for increasing the resolution, e.g. the NAM-WRF model at 4 – 8 km resolution (Janjic 2004).

Hydrologic and meteorological models benefit from ground measurements of surface fluxes for validation and calibration. Eddy covariance (EC) has been the technique of choice for accurate turbulent surface heat flux measurements in the atmospheric surface layer with hundreds of systems installed nationwide (e.g. Katul et al., 1999). An EC system typically consists of a 3D sonic anemometer operated at 10 Hz or faster and a scalar sensor in close proximity (Fig. 1). The kinematic sensible heat flux is then obtained directly from covariances of fluctuations in the vertical velocity w and temperature T. However, several non-trivial corrections have to be applied to the measurements (e.g. Lee et al. 2004) and even then turbulent fluxes from EC systems are typically

10-30% smaller than the available energy, i.e. the difference of net radiation and soil heat flux, an issue known as energy balance non-closure which has yet to be resolved (Wilson et al. 2002; Foken et al. 2006; Twine et al., 2000).

Since EC is a point measurement, the source area or footprint of the measurements is highly variable, depending mostly on wind direction and atmospheric stability (Schmid and Oke 1990, Horst and Weil 1992, Hsieh et al 2000, Schuepp et al. 1990). Over natural surfaces, which always display some degree of heterogeneity, this together with the uncertainties described above leads to noisy and uncertain timeseries of EC turbulent heat fluxes, even for long (30 minute) averaging intervals (e.g. Fig. 5).

The most significant drawback for EC systems, however, is the scale gap between the flux footprint and pixel or grid cell size in hydrologic and meteorological modeling. For tall vegetation, EC systems are typically installed just above the top of the vegetation (i.e. below the top of the roughness sublayer) for reasons of cost, accessibility, and to limit the footprint area to a homogeneous area. While this assures the representativeness of the measured fluxes to the immediate environment of the tower (where also the non-turbulent flux components of the energy balance, net radiation and soil heat flux, are measured), this results in small footprint sizes. For example, Hong (2008) – in a comprehensive study for 12 riparian EC sites in NM, CA, and AZ at the Landsat overpass time (late morning) using the footprint model by Hsieh at al. (2000) - found that the maximum contribution to the footprint is typically within 50m from the tower and 80% of the integrated footprint density function is located within 100m from the tower (Fig. 1).

Thus, the validation and data assimilation of sensible and latent heat fluxes into hydrologic and meteorological models is complicated by the scale gap between footprints of existing surface flux measurement and the pixel or gridcell area of these models (Li et al., 2008, Fig. 1). Meijninger et al. (2002) and Beyrich et al. (2002) recently demonstrated that scintillometry allows the measurements of sensible heat fluxes H at footprint dimensions from 500 to 10,000 m or areas comparable with several pixels of a satellite image (tens of Landsat thermal pixels or a few MODIS thermal pixels). The objective of this paper is to present "lessons learned" from our first-of-its-kind network of seven scintillometers in semi-arid New Mexico (Table 1). In this study, we use SEBAL for estimation of regional H and ET distributions since we are familiar with it. However, any energy balance model or algorithms could be validated by scintillometer measurements

SCINTILLOMETRY: INSTRUMENTATION AND THEORY

A scintillometer transect consists of a transmitter and a receiver (Figs 2 and 3) separated by the transect length L. The receiver measures the intensity fluctuations ("scintillations") in the modulated radiation emitted by the transmitter. These fluctuations are caused by refractive scattering by temperature T and water vapor concentration q variations in turbulent eddies. The variance of the natural log of beam intensity $\sigma_{\ln I}^2$ is proportional to the structure parameter of the refractive index, C_n^2, a measure of "seeing" in the atmosphere.

$$C_n^2 \propto \sigma_{\ln I}^2 D^{7/3} L^{-3} \qquad (1)$$

For the optical (sensible heat flux) large aperture scintillometer (LAS, wavelength 880nm, aperture diameter D = 0.15 m) temperature fluctuations along the path caused by turbulent eddies on the order of D are the primary cause of refractive scattering. Thus the structure parameter of temperature C_T^2 can be deduced from C_n^2. Using Monin-Obukhov similarity theory in the atmospheric surface layer, surface fluxes of sensible heat H, and momentum can be determined iteratively from C_T^2 and supplemental meteorological measurements (e.g. Hartogensis et al. 2003)

$$\frac{C_T^2 (z_{eff} - d)^{2/3}}{-H / \rho c_p u_*} = f_T \left(\frac{z_{eff} - d}{L_{MO}} \right), \qquad (2)$$

where f_T are universal stability correction functions for unstable and stable conditions, respectively (de Bruin et al. 1993). c_p is the specific heat at constant pressure, ρ is the density of air, and L_{MO} is the Obukhov length. The friction velocity u_* is derived from surface roughness parameters and the integrated flux profile relationships (Panofsky and Dutton 1984), and measurements of the mean horizontal wind speed. Over non-flat surfaces, the effective beam height z_{eff} is computed as a weighted average of GPS (or, even better, DGPS) readings of the underlying landscape. Accurate calculation of z_{eff} is complex, but critically important since a relative error in z_{eff} will result in at least half that relative error in H (Hartogensis et al. 2003).

At first, it seems like a large number of parameters are required to derive H from C_T^2 which if they needed to be determined as a representative average over the LAS transect would require a lot of additional measurements and introduce uncertainty. However, assuming typical measurement errors Hartogensis et al. (2003) showed that a single measurement of wind speed, temperature, and pressure near the transect center is sufficient to reduce the error in H to 10% or less. The major contributor to this error is GPS related uncertainty in z_{eff} (6.7%), accurate measurement of path length L (1.4%), wind speed (0.6%) and roughness length (0.4%) are also important, whereas pressure and temperature errors have negligible effects. The relative contributions of these errors change with transect geometry and meteorological conditions. In free convective conditions - often encountered in the southwestern US - u_* (and thus wind speed and roughness length) are no longer needed to calculate H.

$$H_{fc} = 0.48 \rho c_p \left(z_{eff} - d\right) C_T^{6/4} \left(g / T\right)^{1/2} \tag{3}$$

Since similarity theory is used in the derivation of H (Eq. 2&3), surface homogeneity over the footprint area is required and horizontal flux transport and storage fluxes should be zero. However, Meijninger et al. (2002) and Beyrich et al. (2002) demonstrated that a LAS sensible heat flux over a chessboard pattern of crop matched the weighted average of the individual crop H measured by EC. They argued that the LAS beam should be located above the blending height (Bou-Zeid et al. 2004) of individual heterogeneities for similarity theory to hold. For a full description of LAS theory and applications see Hill (1992), Andreas (1990), and the special issue of Boundary-Layer Meteorology “Recent Developments in Scintillometry Research” (de Bruin et al. 2002).

Loescher et al. (2005) and Kleissl et al. (2008), respectively, examined EC and LAS flux measurement consistencies through instrument intercomparisons. Linear regressions for H of eight EC instruments in neutral and unstable stability conditions revealed differences of up to 30%, while typical differences (measured by the standard deviations of the slopes) were 7-11% depending on atmospheric stability. A study with five LASs under ideal conditions in New Mexico showed differences in the regression slopes of up to 21% with typical differences of 5-6%. In these studies great care was taken during installation and maintenance of the equipment, data processing, and site selection. Larger errors may occur in non-ideal conditions.

Whereas typical EC footprints are on the order of 100s of m^2 and cover completely different areas when the wind direction changes more than 90 degrees, the footprint areas of scintillometers are typically on the order of km^2 and cover –at least partly– the same area when the wind direction changes more than 90 (but less than 180) degrees. Since the LAS measurements represent line-averaged measurements weighted towards the center of the transect (Fig. 4), the footprint typically takes the shape of an ellipsoid whose major axis is ~30% less than the actual transect length. A comparison of measurements from five collocated LAS transects and an eddy covariance station reveal that LAS measurements follow the same trend as EC and capture better the effect of short time transient events such as caused by scattered clouds (Fig. 5).

SCINTILLOMETER NETWORK IN NEW MEXICO

The scintillometer network in New Mexico (NMTLASNet) is located within and around the Middle Rio Grande Basin. It consists of seven Kipp & Zonen LAS transects and associated meteorological stations at different locations representing a range of elevations (1448 – 3206 m MSL) and land surfaces: dry homogeneous shrub and grasslands, heterogeneous moist riparian areas, moist homogeneous grassland, homogenous lava flows, and homogeneous irrigated alfalfa fields (Table 1, Figures 6-7). The principal objectives for our current LAS network are: (1) Develop efficient operating procedures and wireless infrastructure for the operation of LASs over a large region; (2) Estimate typical footprint sizes and measurement errors of LAS observations (3) Develop procedures for the use of H measurements by LASs for the calibration of remote sensing algorithms.

Setup and Operating Procedures

The optimal transect is parallel to the earth's surface and perpendicular to the predominant wind direction to have a maximum uncorrelated source area. It should follow a north-south orientation to avoid damage of the optical parts by direct sunlight under low sun angles. For typical transects of 3 km the effect of the curvature of the earth on z_{eff} is less than 0.2 m (Hartogensis et al. 2003). z_{eff} should be within the atmospheric surface layer (ASL) where Monin-Obukhov Similarity Theory (MOST) can be applied to derive H from C_T^2 (Eq. 2). The base of the ASL is two to three times the typical height of the obstacles on the land surface (depending on the density of the obstacles). Thus, the minimum z_{eff} ranges from 1 m over grassland to tens of meters for trees. The maximum height is the top of the ASL, which is on the order of 100 m in daytime, and 10s of meters at night (Brutsaert 1982).

The minimum height is not only determined by the height of the roughness sublayer but also by the phenomenon of "saturation". When C_n^2 increases above a certain threshold, $\sigma_{\ln I}^2$ remains constant (it is 'saturated') and is thus no longer proportional to C_n^2. This violates the assumptions in Eq. 1, and results in an underestimation of H (Clifford et al. 1974). Note that while H is constant in the ASL, C_n^2 decreases with height. Smaller z_{eff} and longer transects lead to more intense scintillations (larger $\sigma_{\ln I}^2$) and more saturation (Eq. 1). For example, to measure H = 400 W/m^2 over a path length of 2750 m, the height of the LAS must be greater than 30 m whereas H = 200 W/m^2 would require a height of at least 10 m (Kipp&Zonen 2007).

Unlike with EC, the locations of LAS transmitter and receiver do not have to be representative for the area under investigation as the measurement is most sensitive at the center of the transect. Thus, to avoid the construction and vibration problems of tall towers, LASs can be set up near the ground across a valley or between two hills. Where such landscape features cannot be found vertically slanted paths can be used. Since LAS beam heights then vary along the path, the LAS measurements not only represent a horizontal but also a vertical average of C_T^2. Table 1 shows that with the exception of the Valles Caldera all our LAS transects have slanted paths where the height difference exceeds 5 m. Advantages of slanted transects are reduction in installation cost and flexibility. The disadvantage is an uncertainty in the derived H which increases with the ratio of maximum to minimum height of the beam. While uncertainty in the physical height of the beam over the transect can be eliminated by careful elevation measurements using differential GPS, the uncertainty caused by different methods for determining the z_{eff} remains. (Hartogensis et al. 2003).

Footprints of LAS measurements

For ground-truthing and data assimilation, it is essential to compare satellite or model results to LAS measurements *over identical areas*. This includes estimating a footprint weighting function of the flux measurement on the ground, summing up the footprint weights within each model grid cell or remote sensing pixel, and computing the weighted average of the model or remote sensing H values over the pixels comprising the footprint. Based on 13 daytime footprints (one example is shown in Fig. 4), we found that the average footprint area [1] was 3.3 km^2.

Several uncertainties plague footprint-averaged statistics: Firstly, footprint calculations are based on turbulence models and use measurements with inherent uncertainty (e.g. wind direction). Secondly, the temporal scale over which the remote sensing image is taken (seconds) is discrete and different than the 10 minute average of the LAS measurement. Thirdly, subgrid-scale (or subpixel scale) heterogeneity within the model gridcell or satellite image pixel is not considered. Subpixel-scale heterogeneity becomes especially important when there is a strong gradient of footprint weights within a pixel. Then the footprint-weighted pixel-averaged value from the LAS is not representative for the relative weighting of the footprint area within that pixel.

Since the 1st issue is also affected by the 3rd (if H was homogeneous over the area comprising the actual and the calculated footprint, then errors in the footprint location would not matter) we examine the effect of subpixel-scale heterogeneity on the heat flux using Landsat-SEBAL H maps on June 16, 2002. Subpixel scale variability is related to features of the landscape and cannot be described with purely statistical approaches (Fig. 8). For example, in the Rio Grande riparian corridor, the river coexists with patches of riparian trees (e.g. Saltcedar and Cottonwood), interdispersed shrubs and grasses, alfalfa fields, and bare, sandy or rocky soil on the edges bordering the desert. This small-scale patchwork changes on scales much smaller than 1 km and leads to significant subpixel-scale variability both in absolute (Fig. 8 left) and relative terms (Fig. 8 right). High subpixel scale variability also occurs at interfaces between different landscapes (so-called ‘mixed pixels’), such as the dry riverbed of the Rio Puerco (upper left corner of the figure),

[1] The footprint area is defined as the area that comprises 95% of the total footprint weight.

and the edge of the mountains (center right). In the desert area (northern half of Fig. 8) the absolute subpixel scale variability is 10% or less.

To quantify the effect of MODIS subpixel scale variability on validation and calibration of remote sensing models, we applied the LAS footprint weighting functions on Sep 17, 2006 1040h LST (the MODIS overpass time) to the 30 m pixel Landsat data (H_{30m}, Fig 9a), and to the aggregated 1 km pixel Landsat data (H_{1km}, Fig. 9b). The Landsat scene covers 4 sites: San Acacia Riparian (SAR), San Acacia Alfalfa (SAA), Sevilleta NWR desert, and EMRTC desert (Table 1). For the more homogeneous desert sites, the differences in H_{30m} and H_{1km} are less than 3% (not shown). However, for the SAR site H_{30m} = 157 Wm^{-2} and H_{1km} = 177 Wm^{-2}, while we obtained H_{30m} = 96 Wm^{-2} and H_{1km} = 171 Wm^{-2} for the SAA site (Fig. 9). While the difference between H_{30m} and H_{1km} at SAR is acceptable, the error at SAA is 78%. From Fig 9b it is obvious that a substantial part of the SAA footprint is over a 'mixed pixel' (the green pixel on the right), which covers partially irrigated riparian area and partially a dry rocky hill. While the majority of the large weights in the footprint are located over the riparian area (Fig. 9a), the mixed pixel artificially increases H_{1km} for the east end of the footprint, leading to overestimation of H_{1km} .

LASs for the calibration and validation of remote sensing algorithms

The primary goal for our LAS network is calibration of the SEBAL remote sensing algorithm to derive maps of sensible and latent heat fluxes over the state of New Mexico operationally in near-real time. The required calibration of H to surface temperatures through user-based selection of a 'hot' (with maximum sensible heat flux) and a 'cold' (with zero sensible heat flux) pixel prevents automatic generation of these maps with SEBAL (Bastiaansen et al. 1998).

LAS sensible heat fluxes could be used to calibrate SEBAL surface temperature to H at the LAS sites and then applied to the entire image.

To evaluate the accuracy of such a calibration procedure we compare SEBAL user-calibrated maps of H on September 17, 2006 (Fig. 10) and 3 other dates (Fig. 11). Figure 10 shows that the SEBAL results generally agree with the 10 min averaged surface LAS measurements at the overpass time, however, particularly the SAA, Sevilleta NWR desert, and VCNP estimates display considerable errors. As discussed earlier, at SAA subpixel scale variability (Fig 9a) is probably responsible for the error. The poor agreement between SEBAL and LAS at the more homogeneous Sevilleta desert site is surprising and requires further research.

Application of SEBAL in the mountains (such as VCNP) is challenging. It is not clear yet whether the difference between LAS and SEBAL there is caused by a biased SEBAL estimate of H, erroneous estimate of the adiabatic lapse rate for the estimation of an elevation corrected surface temperature in the high mountains, or errors in the ground measurements.

LESSONS LEARNED AND CONCLUSIONS

The installation of the NMTLASNet was completed in September 2006 (Table 1). We want to share our "lessons learned" with colleagues who have an interest in employing the novel technology of scintillometry.

The length of a LAS transect strongly depends on the height of the laser beam above the soil surface and the expected maximum H. The commonly reported maximum transect length of 5000 m for a LAS is overly optimistic for natural ecosystems. For New Mexico conditions with maximum

H>400 W/m^2 a maximum transect length of 3000 m is more realistic if the beam height can be maintained at 30 m. These lengths result in footprint areas which are not significantly larger than a MODIS thermal pixel causing difficulties in comparison of LAS and satellite measurements in heterogeneous environments. Downscaling MODIS 1km^2 thermal pixels using 250x250 m MODIS visible and near-infrared data would provide a better resolution for SEBAL calibration and validation. However, transects over homogeneous areas are preferred as uncertainties in the footprint model, meteorological data, and sub-1km-pixel scale variability can accumulate to substantial errors.

From our extensive practical experience with LAS we can attest to the fact that they are easier to operate and more robust than EC systems. Nevertheless new LAS users can avoid pitfalls and become professional operators through training and guidance from an expert. Once a LAS is setup, one site visit every two months is sufficient to service the instrument. Proper functionality can be easily confirmed by observing a single variable – the receiver mean signal strength - that may weaken due to power outages or sudden or creeping misalignment between transmitter and receiver. For example, temporary installations on tripods, cinder blocks without a strong foundation may cause misalignment problems to occur e.g. after heavy rainfall due to soil erosion or settling. Misalignment increases the sensitivity of the measurements to tower vibrations which can introduce additional variance in the signal strength leading to overprediction of H. LAS quality control can be performed easily by a dedicated undergraduate student, whereas quality control of EC systems typically requires the experience of an advanced PhD student. Scintillometer users should consult the manual of their system for installation requirements, but generally a datalogger with the ability for differential voltage measurements, a low bandwidth unidirectional data transmission system for

20 kB/day of uncompressed 10 minute averaged data, and 10W power system should suffice. Unlike with EC systems, storage of high-frequency data is not required, but power spectra of the signal strength may help in detecting vibration issues (van Radow et al. 2008).

It is somewhat more challenging to obtain the full diurnal cycle of H from an automatized data processing algorithm. Since LASs measurements do not give information about the direction of the flux, local minima in C_T^2 need to be found to determine the cross-over from negative to positive and positive to negative heat fluxes around sunrise and sunset, respectively. Temperature measurements at 2 heights can provide information about the direction of the flux more reliably, especially over areas prone to horizontal advection of heat in the afternoon.

Lastly we would like to point out some disadvantages of LAS compared to EC. EC is based on a simple theory to measure the fluxes directly. No additional specifications of the roughness of the surface or the stability of the atmosphere are required. EC systems provide a greater wealth of micrometeorological data than LASs such as velocity variances and momentum fluxes in all directions. After more than 30 years of continuous and widespread use and development the engineering of EC sensors is more advanced than that of LASs.

In summary, in New Mexico we have demonstrated how LAS networks can provide valuable data for hydrologic modelers. We are in the process of optimizing our network based on the experiences described in this paper and upscaling our network to the regional level (1000s km) covering the southwestern USA and Latin America to investigate how scintillometry can contribute to the validation and calibration of remote sensing algorithms, hydrologic models, and NWP. Whereas in New Mexico evaporation is limited by water availability, in the humid tropics of

Panama and Colombia evaporation is limited by available energy except for short periods without precipitation. Two LAS transects will be installed at the Gamboa Tropical Hydrology Observatory (wet) and the “arcos seco” (dry arc) of Panama and one at an elevation of 2500 m in the highlands surrounding Medellin, Colombia. We are actively looking for sponsors to cover the operating expenses of the network and mesoscale meteorologists and hydrologist who would be interested in the data for modeling or data assimilation.

ACKNOWLEDGEMENT

The following persons provided property or otherwise invaluable assistance in establishing field sites: Jesus Gomez, Whitney Defoor, and Kimberly Bandy (all sites); Don Natvig and Renee Brown (Sevilleta National Wildlife Refuge); Herschel Schulz (Chief Ranger, El Malpais National Monument); Corky Herkenhoff and David Morris (San Acacia Alfalfa); Lorenzo Benavides (San Acacia Riparian); Dan Klinglesmith (Magdalena Ridge); Bob Parmenter (Valles Caldera National Preserve). The following sponsors have contributed to this study: USGS-NIWR USGS award number 06HQGR0187 and NMSU-WRRI contract Q01112, NSF EPSCoR grant EPS-0447691; U.S. Department of Agriculture, CSREES grant No.: 2003-35102-13654; NASA Cooperative Agreement NNA06CN01A; the NSF Science and Technology Center program Sustainability of Semi-Arid Hydrology and Riparian Areas (SAHRA; EAR-9876800).

REFERENCES

Allen, R.G., M. Tasumi, and R. Trezza, 2007, Satellite-based energy balance for mapping evapotranspiration with internalized calibration (METRIC) – Model. *J. Irrigation and Drainage Engineering,* **133** (4): 380-394.

Andreas, 1990, Selected Papers on Turbulence in a Refractive Medium. SPIE Milestone Series, International Society for Optical Engineering, **25**, 693 pp.

Anderson, M.C., J.M. Norman, J.R. Mecikalski, R.D. Torn, W.P. Kustas, and J.B. Basara. 2004. A multi-scale remote sensing model for disaggregating regional fluxes to micrometeorological scales. *J. Hydrometeorology*, **5**, 343-363.

Bastiaanssen, W.G.M., M. Menenti, R.A. Feddes, and A.A. M. Holtslag. 1998, A remote sensing surface energy balance algortithm for land (SEBAL). Part 1: Formulation. *J. of Hydrology*, 198-212.

Beyrich, F., H.A.R. De Bruin, W.M.L. Meijninger, J.W. Schipper, and H. Lohse., 2002, Results from one-year continuous operation of a large aperture scintillometer over heterogeneous land surface. *Bound.-Layer Meteorol.*, **105**, 85-97.

Bou-Zeid E., C. Meneveau, M.B. Parlange, 2004, 'Large-eddy simulation of neutral atmospheric boundary layer flow over heterogeneous surfaces: Blending height and effective surface roughness,' *Water Resources Res.*, 40(W02505), doi:10.1029/2003WR002475.

Brutsaert W.H., 1982, Evapotranspiration into the Atmosphere, Theory, History and Applications, Reidel Publising Co., Boston.

Choudhury, B.J., 1989, Estimating evaporation and carbon assimilation using infrared temperature data: Vistas in modeling. In G. Asrar (Ed.), Theory and applications in optical remote sensing. John Wiley, New York, pp. 628-690.

Clifford, S., G. Ochs, and R. Lawrence, 1974, Saturation of optical scintillation by strong turbulence. *J. Opt. Soc. Am.*, **64**, 148– 154.

De Bruin, H.A.R., 2001, Introduction: Renaissance of Scintillometry, *Boundary-Layer Meteorol.*, **105**(1), 1-4.

De Bruin, H.A.R., W. Kohsiek, and B.J.J.M. Van den Hurk, 'A Verification of Some Methods to Determine the Fluxes of Momentum, Sensible Heat and Water Vapour using Standard Deviation and Structure Parameter of Scalar Meteorological Quantities', *Boundary-Layer Meteorol.* **63**, 231-257, 1993

Foken, T., F. Wimmer, M. Mauder, C. Thomas, and C. Liebethal, 2006, Some aspects of the energy balance closure problem, *Atmos. Chem. Phys. Discuss.*, **6**, 3381–3402.

Goodrich D.C., R. Scott, J. Qi, B. Goff, C. L. Unkrich, M. S. Moran, D. Williams, S. Schaeffer, K. Snyder, R. MacNish, T. Maddock, D. Pool, A. Chehbouni, D. I. Cooper, W. E. Eichinger, W. J. Shuttleworth, Y. Kerr, R. Marsett and W. Nil, 2000, Seasonal estimates of riparian evapotranspiration using remote and in-situ measurements, *Agric. Forest Meteorol.*, **105**(1-3), 281-309.

Hartogensis, O.K., C. J. Watts, J.-C. Rodriguez, H.A.R. De Bruin, 2003, Derivation of effective height for scintillometers: La Poza experiment in Northwest Mexico. *J. Hydrometeorology*, **4**, 915-929

Hendrickx, J.M.H., and S.-H. Hong. 2005, Mapping sensible and latent heat fluxes in arid areas using optical imagery. *Proc. International Society for Optical Engineering*, SPIE 5811:138-146.

Hill, R.J., 1992, Review of optical scintillation methods of measuring the refractive-index spectrum, inner scale and surface fluxes. *Waves in Random Media*, **2**, 179-201

Hong, S. 2008. Mapping regional distributions of energy balance parameters using optical remotely sensed imagery. Ph.D. Dissertation, New Mexico Tech, Socorro NM.

Horst, T.W. and J.C. Weil. 1992, Footprint Estimation for Scalar Flux Measurements in the Atmospheric Surface Layer. *Bound.-Layer Meteorology.* **59**: 279-296.

Hsieh, C.-I., G. Katul, and T.-W. Chi, 2000, An approximate analytical model for footprint estimation of scalar fluxes in thermally stratified atmospheric flows. *Adv. Water Res.,* **23**, 765-772.

Janjic, Z. L., 2004: The NCEP WRF core. Preprints, *20th Conference on Weather Analysis and Forecasting/16th Conference on Numerical Weather Prediction*, Seattle, WA, Amer. Meteor. Soc., on CD-ROM

Katul, G., C.-I. Hsieh, D. Bowling, K. Clark, N. Shurpali, A. Turnipseed, J. Albertson, K. Tu, D. Hollinger, B. Evans, B. Offerle, D. Anderson, D. Ellsworth, C. Vogel, and R. Oren, 1999: Spatial variability of turbulent fluxes in the roughness sublayer of an even-aged pine forest. *Bound.-Layer Meteorol.*, **93**, 1–28.

Kipp & Zonen, 2007, Large Aperture Scintillometer Instruction Manual

Kleissl, J., J. Gomez, S.-H. Hong, K. Fleming, J.M.H. Hendrickx, T. Rahn, 2008, Large Aperture Scintillometer Intercomparison Study. *Bound.-Layer Meteorol.*, in press.

Kustas, W.P. and J.M. Norman. 1996, Use of remote sensing for evapotranspiration monitoring over land surfaces. *Hydrol. Science J.*, **41**, 495-515.

Lee, X. (Ed.), Massman W. (Ed), Law B. (Ed), 2004, Handbook of Micrometeorology: A Guide for Surface Flux Measurement and Analysis (Atmospheric and Oceanographic Sciences Library). Kluwer Academic Publishers, The Netherlands.

Loescher, H., T. Ocheltree, B. Tanner, E. Swiatek, B. Dano, J. Wong, G. Zimmerman, J. Campbell, C. Stock, L. Jacobsen, Y. Shiga, J. Kollas, J. Liburdy, and B. Law, 2005, Comparison of temperature and wind statistics in contrasting environments among different sonic anemometer-thermometers. *Agricultural Forest Meteorol.,* **133**, 119–139

Meijninger, W., O. Hartogensis, W. Kohsiek, J. Hoedjes, R. Zuurbier, and H. de Bruin, 2002: Determination of area averaged sensible heat fluxes with a large aperture scintillometer over a heterogeneous surface - Flevoland field experiment. *Bound.-Layer Meteorol*., **105**, 63-83

Middle Rio Grande Water Assembly. 1999. Middle Rio Grande water budget (where water comes from, and goes, and how much): averages for 1972-1997. Middle Rio Grande Council of Governments of New Mexico. 10 pages.

Moran, S.M., and R.D. Jackson. 1991. Assessing the spatial distribution of evaporation using remotely sensed inputs. *J. Environ. Qual.,* **20**, 725-737.

Panofsky, H. and J. Dutton, 1984: Atmospheric Turbulence. John Wiley & Sons, New York.

Peters Lidard, C.D., S. Kumar, Y. Tian, J.L. Eastman, and P. Houser. 2004. Global urban-scale land-atmosphere modeling with the land information system. 84th AMS Annual Meeting 11-15 January 2004, Symposium on Planning, Nowcasting, and Forecasting in the Urban Zone.

Scintec, 2004, Boundary Layer Scintillometer: Turbulence, Heat Flux, Crosswind over Large Spatial Scales, http://www.scintec.com/Site.1/turb.htm

Schmid, H.P. and T.R. Oke. 1990, A model to estimation the source area contributing to turbulent exchange in the surface layer over patchy terrain. *Q.J.R. Meteorol. Soc.,* **116**, 965-988.

Schuepp P.H., M.Y. Leclerc, J.I. MacPherson, and R.L. Desjardins, 1990, Footprint prediction of scalar fluxes from analytical solutions of the diffusion equation, *Bound.-Layer Meteorol.*, **50**, 355-373

Song, J., M. L. Wesely, R. L. Coulter, and E. A. Brandes, 2000, Estimating watershed evapotranspiration with PASS. Part I: Inferring root-zone moisture conditions using satellite data. *J. Hydrometeorol.*, **1**, 447–461.

Twine TE, WP Kustas, JM Norman, DR Cook, PR Houser, TP Meyers, JH Prueger, PJ Starks, 2000, Correcting eddy covariance flux underestimates over a grassland. *Agric. For. Meteor,* **103***,* 279-300

Von Randow C., B. Kruijt, A.A.M. Holtslag, M.B.L. de Oliveira, 2008, Exploring eddy-covariance and large-aperture scintillometer measurements in an Amazonian rain forest, *Agricultural and Forest Meteorology*, **148**, 680-690

Wilson, K., A. Goldstein, E. Falge, M. Aubinet, D. Baldocchi, P. Berbigier, C. Bernhofer, R. Ceulemans, H. Dolmanh, C. Field, A. Grelle, A. Ibrom, B. Lawl, A. Kowalski, T.Meyers, J. Moncrieff, R. Monsonn, W. Oechel, J. Tenhunen, R. Valentini, and S. Verma, 2002. Energy balance closure at FLUXNET sites. *Agric. For. Meteorol.*, **113**, 223–243.

FIGURE AND TABLE CAPTIONS

Figure 1: Spatial and temporal scales of measurement (black) and modeling (red) methods: GCM: global circulation model, NAM: North American model, LIS: NASA Land Information System

Figure 2: Two LASs (one receiver and one transmitter of two separate transects) during the LAS intercomparison study in northern New Mexico (Kleissl et al., 2008). The corresponding transmitter and receiver are 2 km away.

Figure 3: Layout of scintillometer system and illustration of turbulent structures that cause beam refraction on density variations (modified from Scintec, 2004).

Figure 4: Footprint weighting function (color, unitless) for a LAS transect (crosses) at the EMRTC site (Table 1) in Socorro, NM, on September 17, 2006 1035h MST. 95% of the footprint weighting function is represented by an area of 5.0 km^2. MODIS thermal pixels are shown as dotted lines.

Figure 5: Intercomparison of sensible heat flux measurements from five LASs (symbols and serial number in the legend), EC (red line), and net radiation (black line) at the VCNP mountain grassland site (Table 1) on June 19, 2006. LASs can capture the effect of short transient events (e.g. cloudiness at 15h) better than EC due to the short averaging time scale.

Figure 6: Examples of LAS setup locations in New Mexico: Upper left: El Malpais lava flows (EMNM); Upper right: San Acacia riparian area (SAR); Lower left: Valles Caldera mountainous grassland (VCNP), lower right: EMRTC dry shrubland near Socorro (Table 1).

Figure 7: Locations of LAS transects in New Mexico in March 2007 overlaid on a MODIS true color image. UTM 13 northing coordinates are shown on the right.

Figure 8: Sub-1km pixel scale variability in the sensible heat flux H based on SEBAL analysis of a 30 m resolution Landsat image on June 16, 2002. Left: Standard deviation of ~1111 30 m pixels within a $1km^2$ area. Right: Coefficient of variation (standard deviation / mean) within the 1km2 pixel. The centers of LAS transects are shown as black crosses.

Figure 9a: 30m SEBAL-Landsat map of sensible heat fluxes near San Acacia in and around the Rio Grande riparian area of New Mexico in UTM13 coordinates. Crosses: LAS transect ends (left: SAA, right: SAR, Table 1). Solid lines: contour lines of footprint weights (the weights decrease by a factor of $10^{1/2}$ per line). Dotted lines show the outlines of 1km pixels

Figure 9b: Same as Fig 9a, but averaged over 1km pixels.

Figure 10: Time series of LAS measured sensible heat fluxes H (top) and global solar radiation (bottom) on Sep 17, 2006. SEBAL estimates at the MODIS overpass time (10:35 LST) are presented with crosses for each site. a) On this sunny day in New Mexico, peaks of H range from less than 100 W/m^2 over an irrigated alfalfa field (SAA) to 400 W/m^2 over low-albedo lava flows (EMNM). Note that the EMRTC cross is right on the purple line and that the Sevilleta (SNWR, red), San Acacia Riparian (SAR, green), and SAA (blue) are on top of each other. b) The solar radiation data show a cloud-free day. Note that SEBAL solar radiation

is calculated perpendicular to the local surface, whereas the measurements show global horizontal radiation.

Figure 11: Scatter plot of LAS and SEBAL sensible heat fluxes at six sites (Table 1) and four satellite overpasses in 2006. The legend shows month, day, and site name.

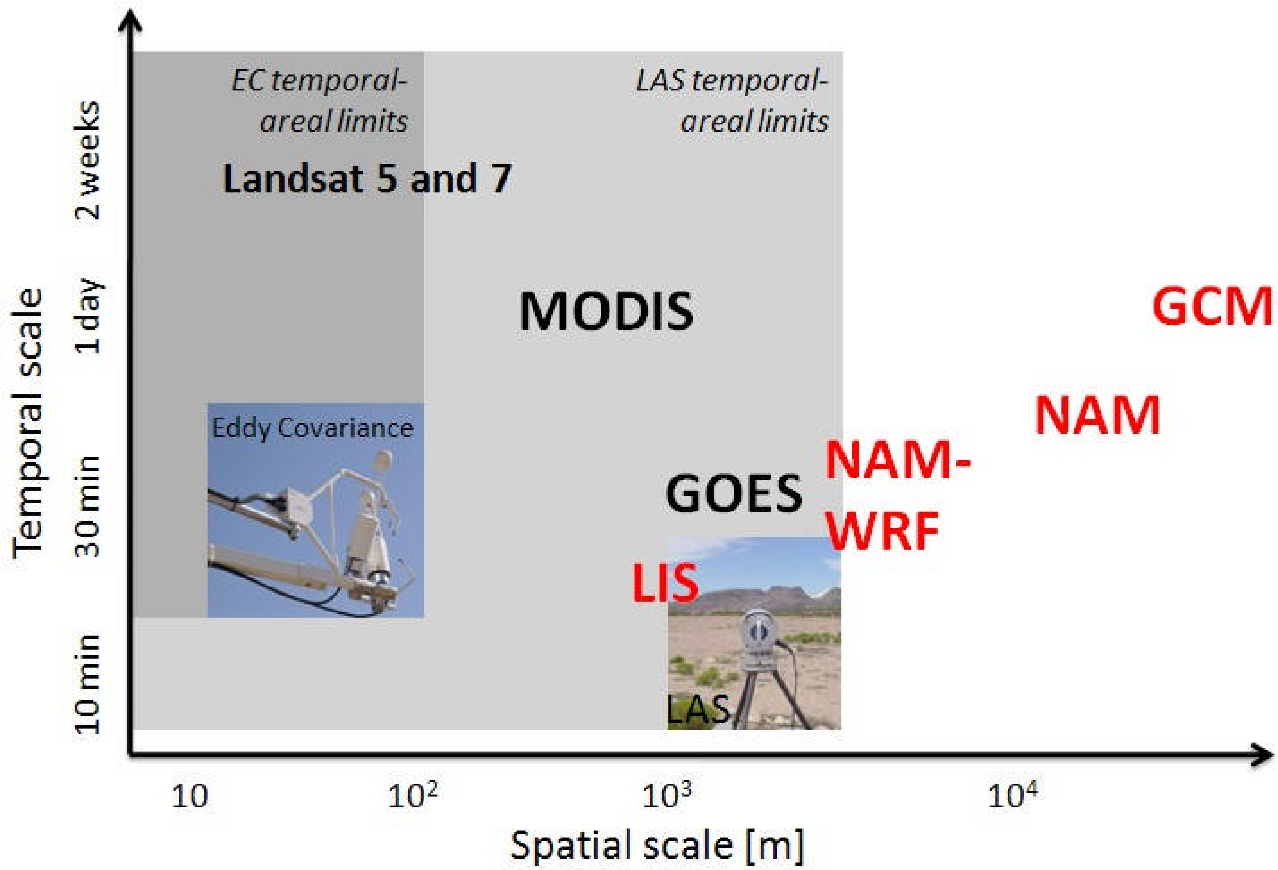

Figure 1: Spatial and temporal scales of measurement (black) and modeling (red) methods: GCM: global circulation model, NAM: North American model, LIS: NASA Land Information System

Figure 2. Two LASs (one receiver and one transmitter of two separate transects) during the LAS intercomparison study in northern New Mexico (Kleissl et al. 2008). The corresponding transmitter and receiver are 2 km away.

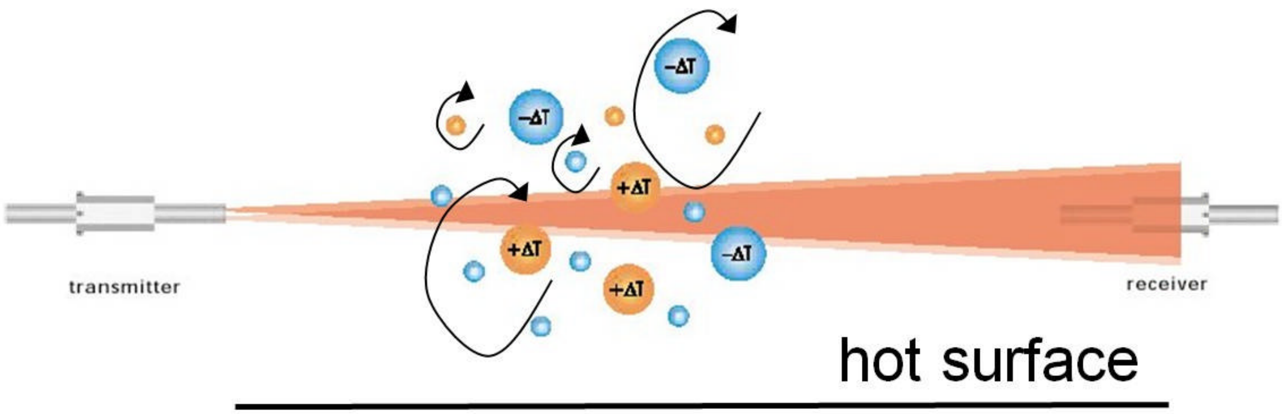

Figure 3. Layout of scintillometer system and illustration of turbulent structures that cause beam refraction on density variations (modified from Scintec, 2004).

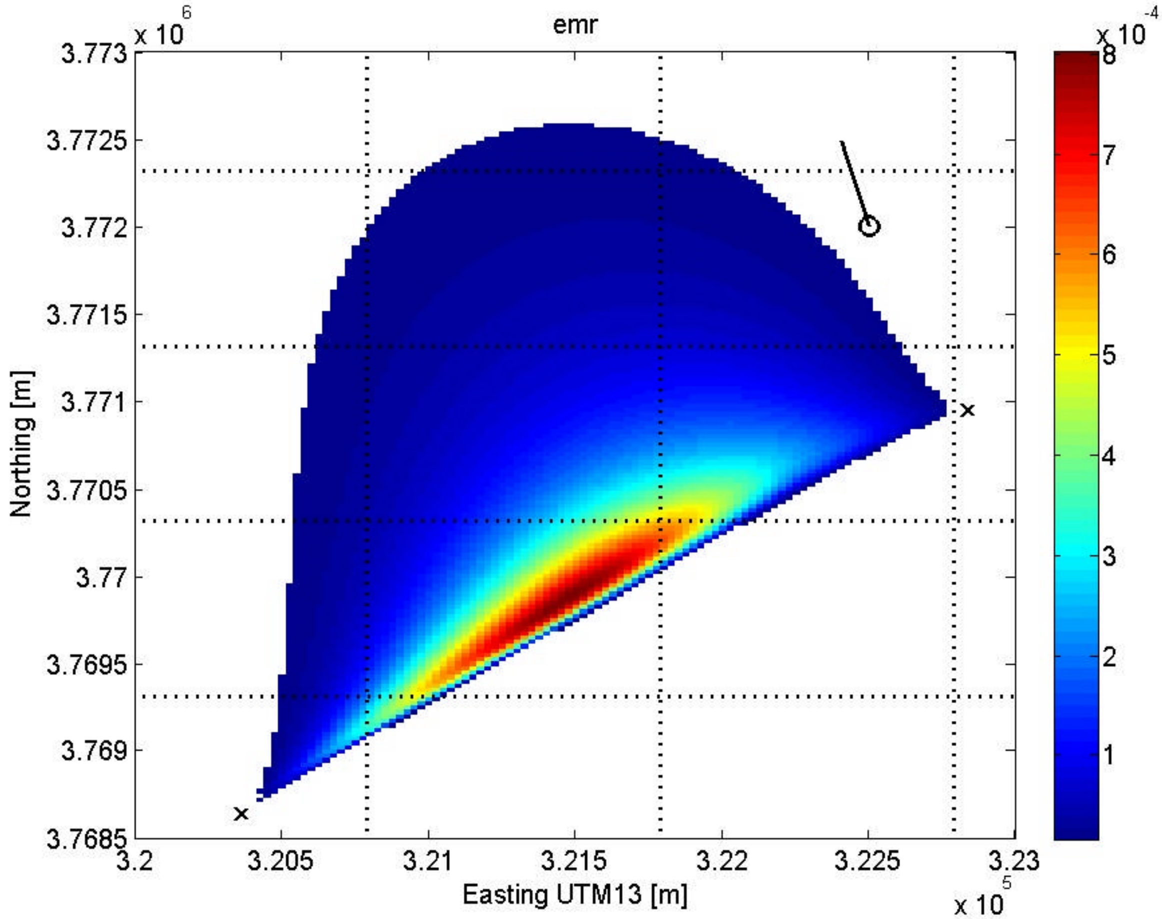

Figure 4. Footprint weighting function (color, unitless) for a LAS transect (crosses) at the EMRTC site (Table 1) in Socorro, NM, on September 17, 2006 1035h MST. 95% of the footprint weighting function is represented by an area of 5.0 km^2. MODIS thermal pixels are shown as dotted lines. The wind direction was north-northwesterly (upper right corner).

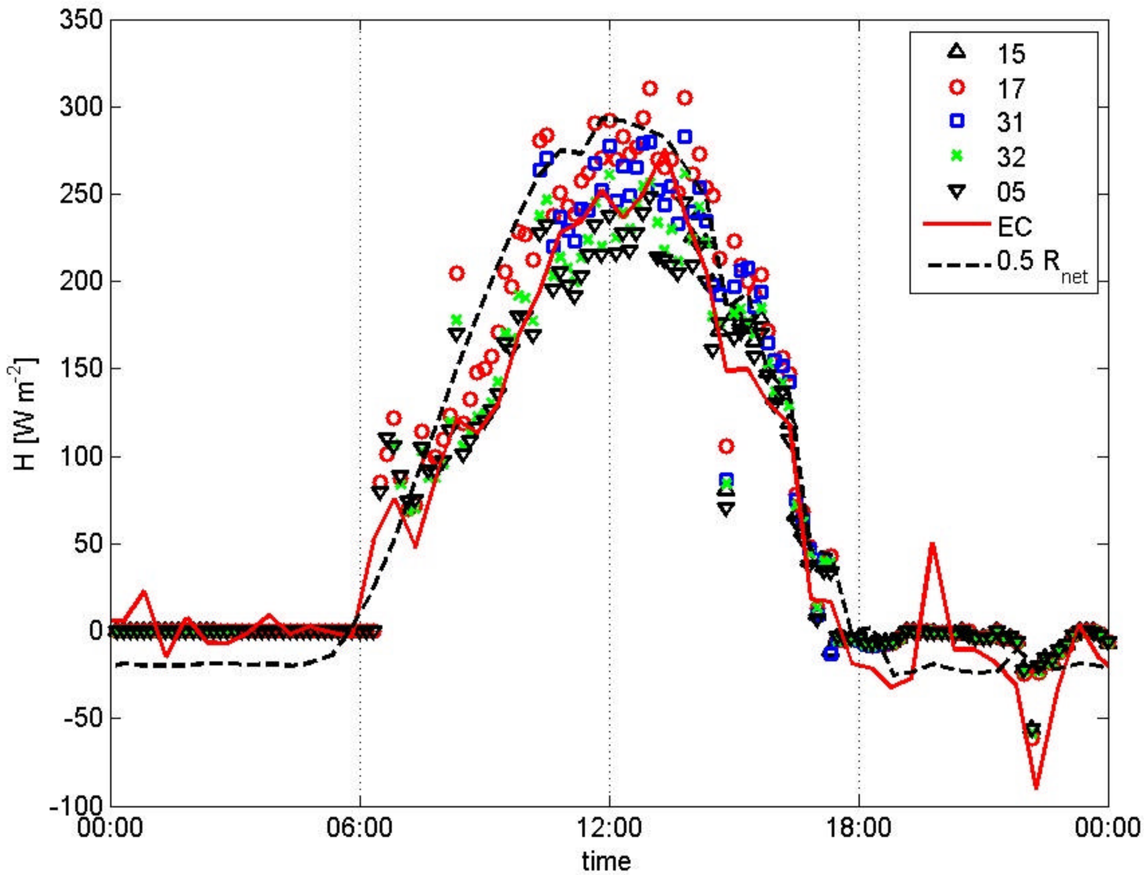

Figure 5: Intercomparison of sensible heat flux measurements from five LASs (symbols and serial number in the legend), EC (red line), and net radiation (Rnet, rescaled by ½, black line) at the VCNP mountain grassland site (Table 1) on June 19, 2006. LASs can capture the effect of short transient events (e.g. cloudiness at 15h) better than EC due to the short averaging time scale.

Figure 6: Examples of LAS setup locations in New Mexico: Upper left: El Malpais lava flows (EMNM); Upper right: San Acacia riparian area (SAR); Lower left: Valles Caldera mountainous grassland (VCNP), lower right: EMRTC dry shrubland near Socorro (Table 1).

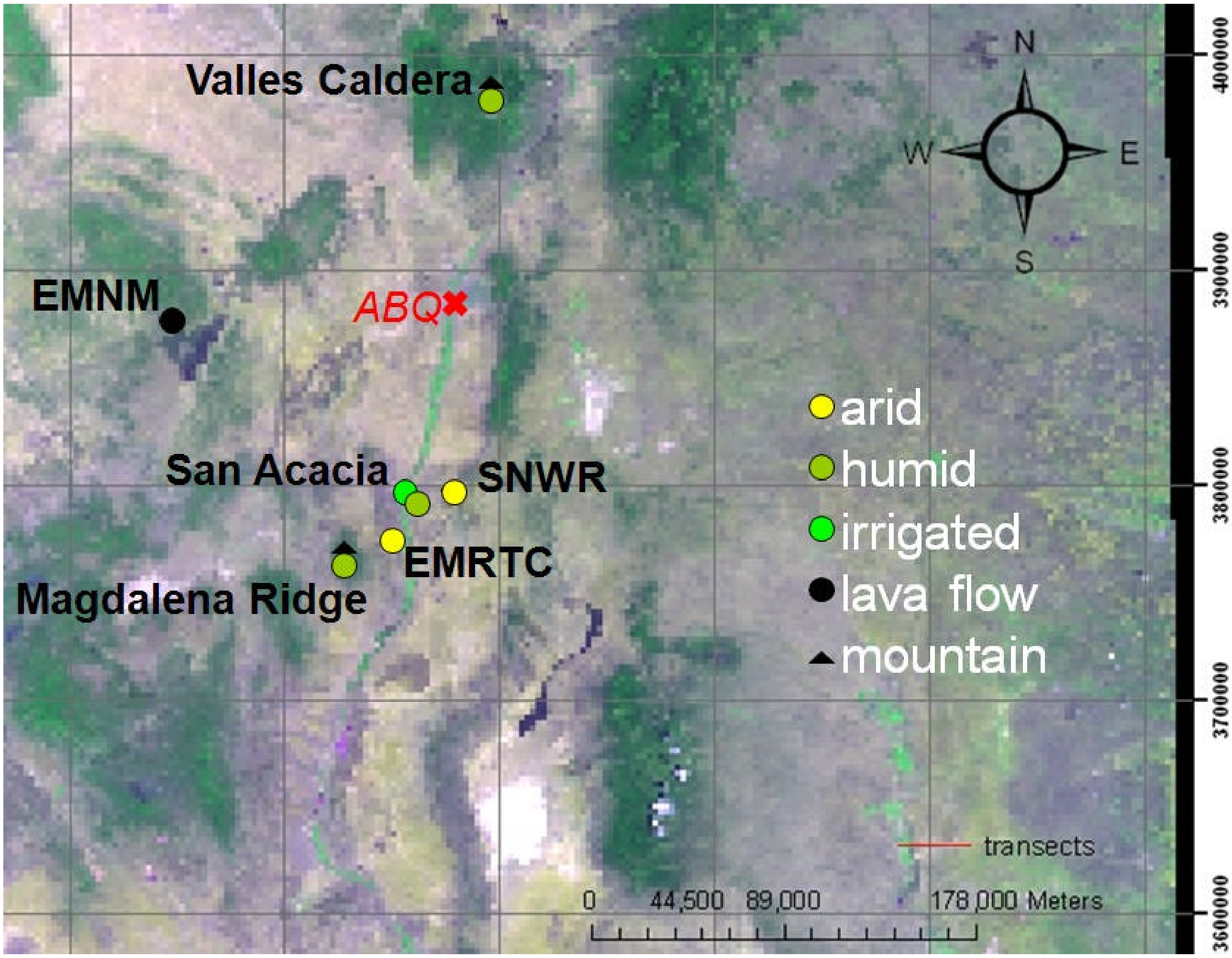

Figure 7

Locations of LAS transects in New Mexico in March 2007 overlaid on a MODIS true color image. UTM 13 northing coordinates are shown on the right. The city of Albuquerque is marked in red. Acronyms can be found in Table 1.

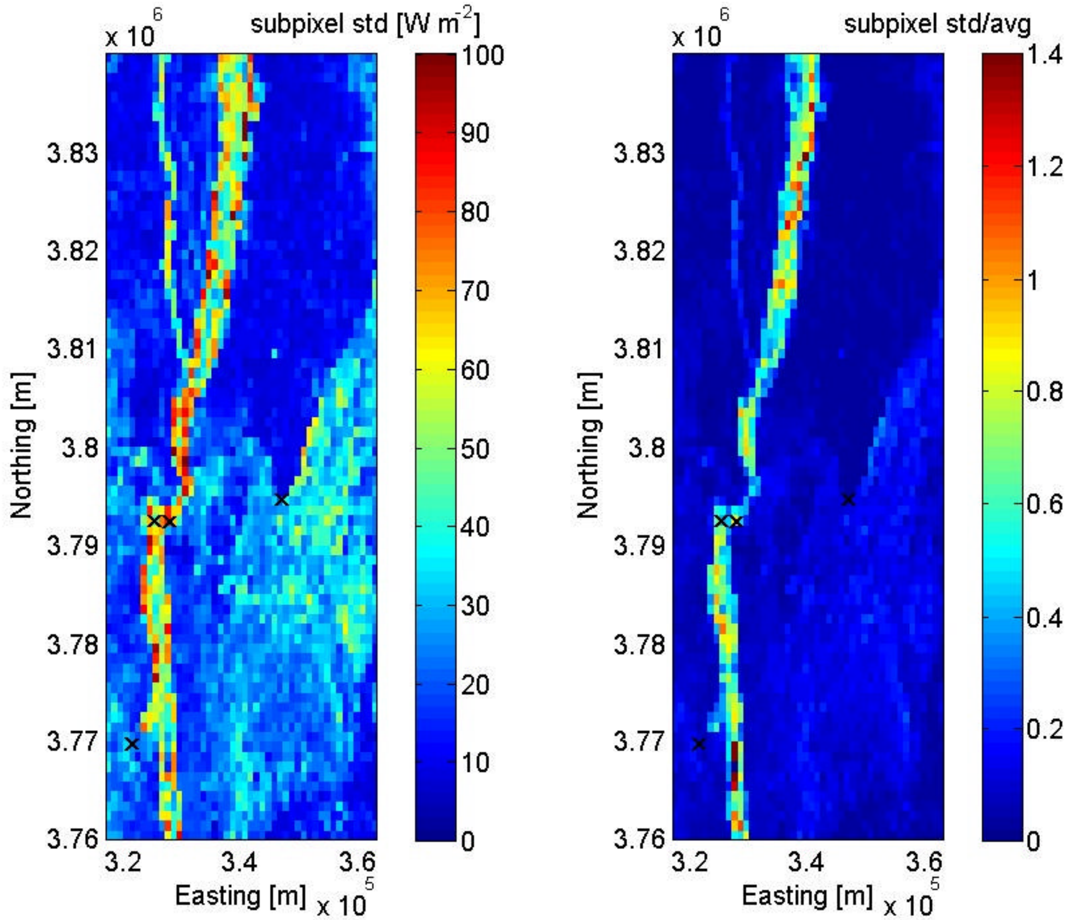

Figure 8: Sub-1km pixel scale variability in the sensible heat flux H based on SEBAL analysis of a 30 m resolution Landsat image on June 16, 2002 at 1030h MST. Left: Standard deviation of ~1111 30 m pixels within a 1km2 area. Right: Coefficient of variation (standard deviation / mean) within the 1km2 pixel. The centers of LAS transects are shown as black crosses.

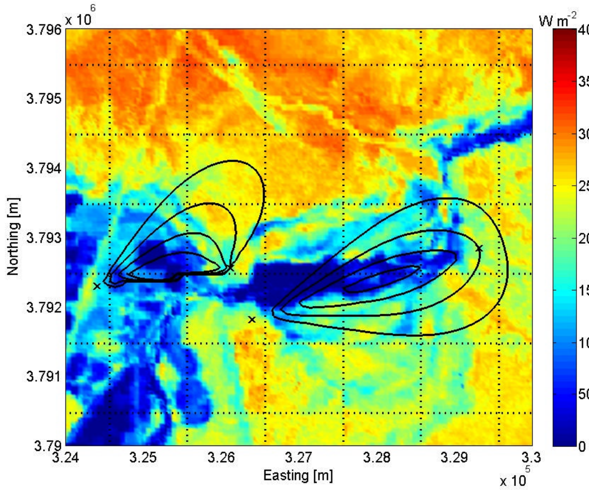

Figure 9a: 30m SEBAL-Landsat map of sensible heat fluxes near San Acacia in and around the Rio Grande riparian area of New Mexico in UTM13 coordinates. Crosses: LAS transect ends (left: SAA, right: SAR, Table 1). Solid lines: contour lines of footprint weights (the weights decrease by a factor of $10^{1/2}$ per line). Dotted lines show the outlines of 1km pixels

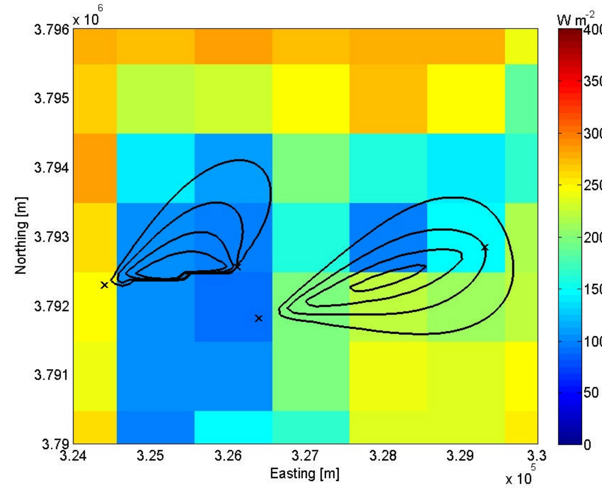

Figure 9b: Same as Fig 9a, but averaged to 1km pixels.

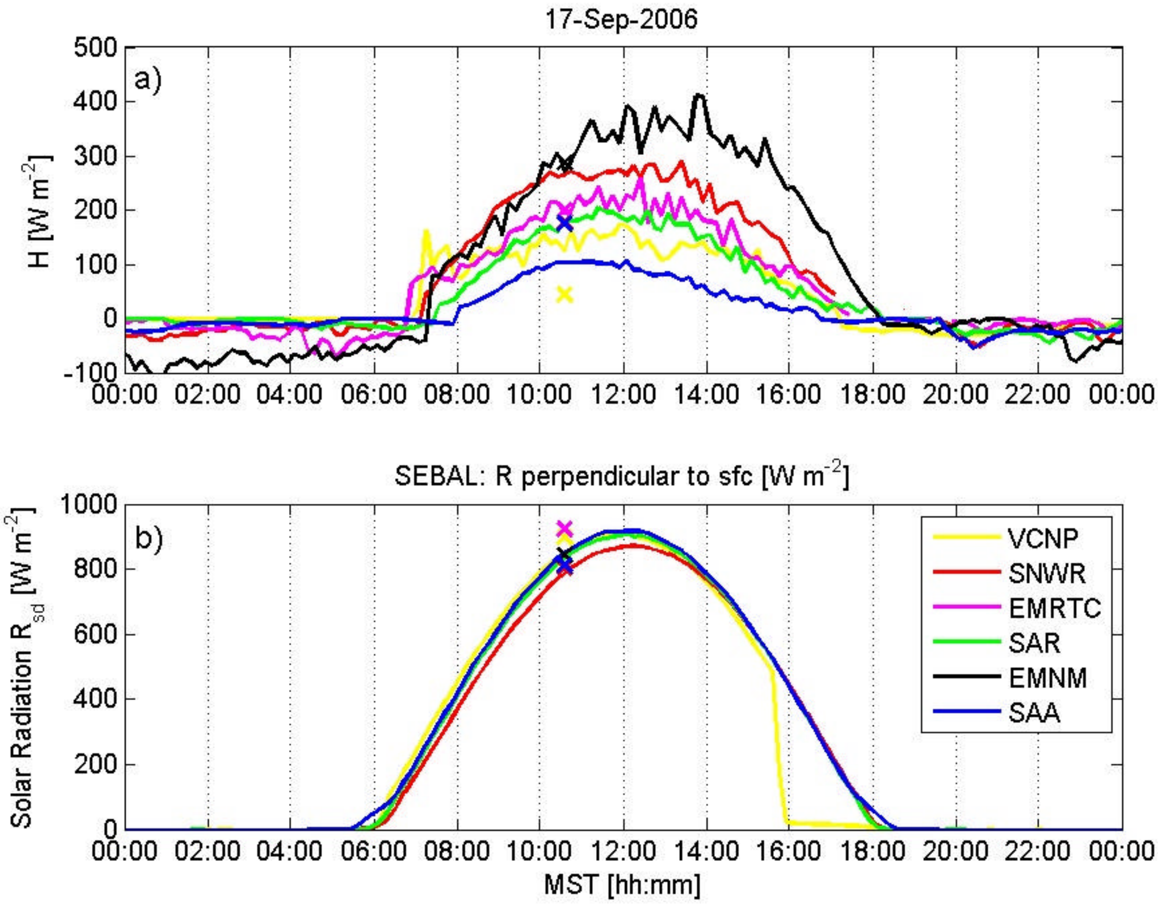

Figure 10: Time series of LAS measured sensible heat fluxes H (top) and global solar radiation (bottom) on Sep 17, 2006. SEBAL estimates at the MODIS overpass time (10:35 LST) are presented with crosses for each site. a) On this sunny day in New Mexico, peaks of H range from less than 100 W/m^2 over an irrigated alfalfa field (SAA) to 400 W/m^2 over low-albedo lava flows (EMNM). Note that the EMRTC cross is right on the purple line and that the Sevilleta (SNWR, red), San Acacia Riparian (SAR, green), and SAA (blue) are on top of each other. b) The solar radiation data show a cloud-free day. Note that SEBAL solar radiation is calculated perpendicular to the local surface, whereas the measurements show global horizontal radiation.

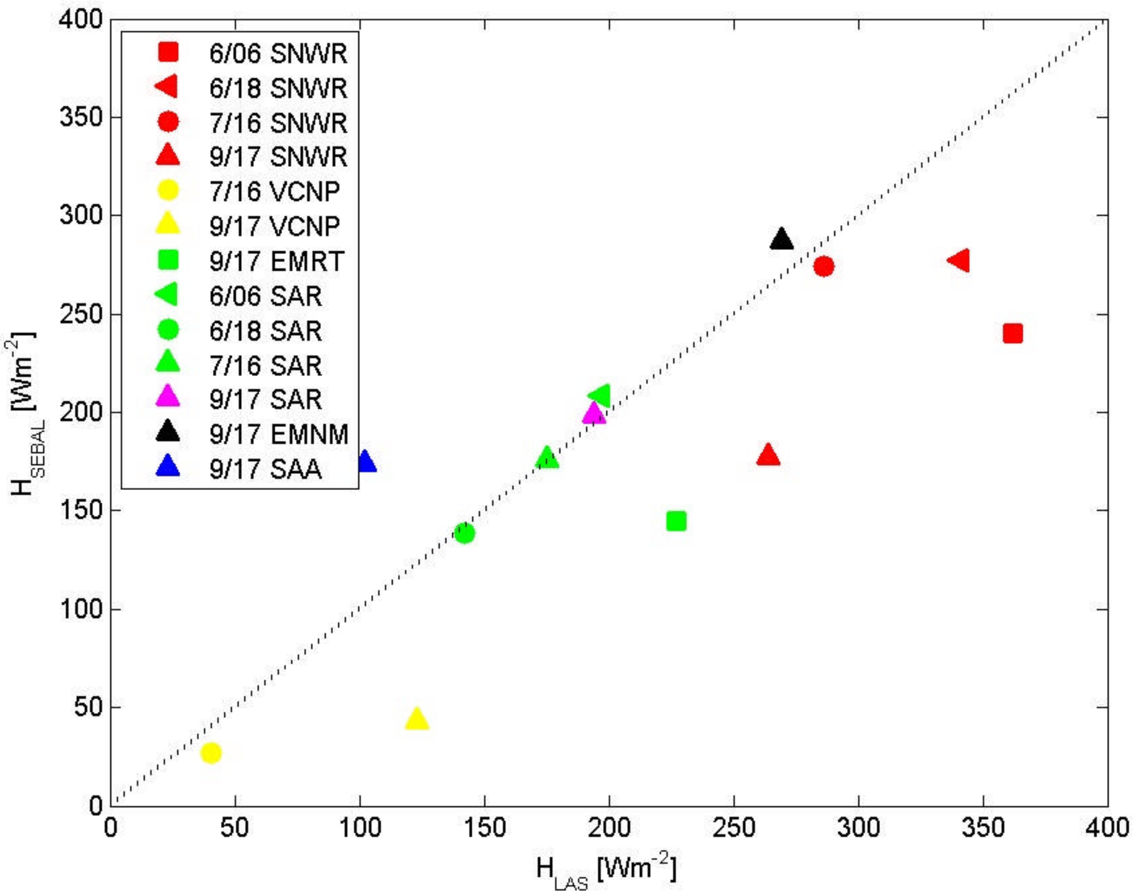

Figure 11: Scatter plot of LAS and SEBAL sensible heat fluxes at six sites (Table 1) and four satellite overpasses in 2006. The legend shows month, day, and site name.

Table 1: New Mexico Tech Large Aperture Scintillometer Network. All coordinates are given in UTM 13, unless otherwise noted. z_o: roughness length, d: zero displacement height. Meteorological sensors: R_{sd}: shortwave downwelling radiation, wspd: wind speed, wdir: wind direction, T: Temperature at 2 m, RH: relative humidity, T_{sfc}: IR surface temperature, EB: Eddy covariance & energy balance, soil: soil temperature, moisture, conductivity. Depending on the representativeness of the receiver location for the transect, the meteorological station is setup there for convenience, or near the center of the transect.

Site	**Sevilleta National Wildlife Refuge (SNWR)**	**San Acacia Riparian (SAR)**	**EMRTC**	**Valles Caldera National Preserve (VCNP)**	**Magdalena Ridge Observatory (MRO)**	**El Malpais National Monument (EMNM)**	**San Acacia Alfalfa (SAA)**
Ecosystem	Dry grassland homogen.	Riparian heterogen.	Dry shrubland homogen.	Grass, mountains homogen.	Grass, mountains heterogen.	Lava flows homogen.	Alfalfa homogen.
z_o | d [m]	.026 | .01	0.31 | 4.14	.03 | .01 (est.)	.014 | .01	not conclusive	.2 | .1 (est.)	variable
LAS Serial No.	050016	050024	050015	060032	030005	060031	050017
Data since	Nov 19, 2005	May 3, 2006	July 18,2006	June 6, 2006	July 23, 2006	Sep 1, 2006	Sep 9, 2006
Receiver: Northing [m]	3795105	3791818	3770951	3972272	3761674	UTM 12! 3876026	3792556
Easting [m]	345711	326400	322835	367312	298177	765019	326121
Elevation [m]	1688	1486	1448	2675	3206	2533	1460
Transmitter: Northing [m]	3794128	3792843	3768646	3972872	3762206	3874340	3792296
Easting [m]	347899	329312	320363	365401	297886	767611	324409
Elevation [m]	1789	1472	1681	2678	3222	2423	1424
Met station: Northing [m]	at Receiver	34.265602 °N	at Receiver	3969278	at Receiver	3875505	3792814
Easting [m]		-106.86776 °W		362649		766108	324999
Elevation [m]		1427		2658		2395	1429
Meteorological Sensors	R_{sd}, wspd, wdir, T/RH, T_{sfc}	R_{sd}, wspd, wdir, T, T_{sfc} **EB tower**	wspd, wdir, T (10cm), soil T/RH, R_{sd}	R_{sd}, wspd, wdir, T/RH, soil, T_{sfc}**, EB tower**	T/RH, T, soil R_{sd}, p, rain	R_{net}, T(.1m), T/RH(2m), wspd, wdir, R_{sd}, T_{sfc}	T_{sfc}, wind wspd, wdir, T/RH, R_{sd}, T_{soil}, rain
Trans. Length [m]	2398	3087	3388	2003	606	2941	1732
z_eff [m]	31.5	44.8	62.9	42.6	17.6	59.8	20.0